Remote Sensing of Environment 264 (2021) 112639

Contents lists available at ScienceDirect

Remote Sensing of Environment

journal homepage: www.elsevier.com/locate/rse

A synergic study on estimating surface downward shortwave radiation from satellite data

Dongdong Wang *, Shunlin Liang, Ruohan Li, Aolin Jia

Department of Geographical Sciences, University of Maryland, College Park, MD 20742, USA

A B S T R A C T

Surface downward shortwave radiation (DSR) is a fundamental variable in determining the Earth's radiation balance and is essential in many applications. Considerable efforts have been devoted to algorithm development, product generation, and validation. However, few studies have focused on comparing retrieval approaches, examining their strengths and weaknesses, and identifying the most suitable scenarios for each approach. In this study, we implemented and evaluated five representative DSR retrieval algorithms, including the forward parameterization approach, two physical inversion methods (look-up table (LUT) and optimization), and two statistical inversion methods (direct estimation and neural networks). We then proposed an algorithm-integration framework that combined the results of these DSR retrieval methods to further improve DSR estimation accuracy and consistency. To validate the DSR retrievals, we used in-situ data collected at 25 stations of the Baseline Surface Radiation Network (BSRN) over one year. Validation revealed that forward parameterization consistently performed best, with an overall root mean square error (RMSE) of 91.7 W/m^2 or a relative RMSE of 16.9%, although it generated the fewest valid retrievals. For an identical data set, the LUT approach generated results comparable to those of parameterization. The neural network-based algorithm-integration approach reduced the RMSE by 11.0 W/m^2 or the relative RMSE by 2.0%, compared to the best individual retrieval algorithm. Our analysis demonstrates that algorithm integration is a promising way to obtain DSR data that are superior to estimates from any individual retrieval algorithm.

1. Introduction

Downward shortwave radiation (DSR) reaching the Earth's land surface is the energy available for terrestrial ecosystem productivity and clean energy production. It controls the exchange of matter and energy at the atmospheric boundary layer, thus governing the cycling of water, carbon, and other elements of great significance to climatic and ecological systems and human society (Liang et al., 2019). Accurate information on the temporal and spatial variability of DSR is essential for studying the Earth's radiation budget (Berbery et al., 1999), hydrological cycling (Huang et al., 2016b), ecosystem productivity (Nemani et al., 2003), agricultural management (de Wit et al., 2005), renewable energy planning (Mellit and Kalogirou, 2008), and many other applications. Remote sensing is currently the only feasible technology for regularly mapping global DSR.

Early attempts to estimate DSR from satellite data were accompanied by the launch of the first generation of Earth observation satellites (e.g., Fritz et al., 1964). Since then, more and more advanced algorithms, based on an accurate modeling of the statistical relationship between satellite data and DSR (e.g., Peng et al., 2020) or on a sophisticated understanding of the physics of atmospheric radiative transfer (e.g., Letu et al., 2020), have been developed and used to generate satellite DSR products. A comprehensive summary of DSR retrieval algorithms can be found in a recent review paper (Huang et al., 2019). The various methods differ in their theoretical basis and conceptual framework, and their performance varies depending on atmospheric and surface conditions. Each method has its own strengths and weaknesses, and is applicable in specific scenarios. Comparing different retrieval algorithms is essential for algorithm selection as well as for algorithm integration to leverage the strengths of multiple retrieval algorithms.

As an indirect measuring approach, validation is essential in satellite DSR retrieval algorithm development and product generation to ensure product accuracy and stability for data users and to provide diagnostic information for product refinement and improvement. Validation is usually conducted during algorithm development (Wang and Pinker, 2009). The stand-alone assessment of multiple products by data developers or independent researchers is not uncommon (Zhang et al., 2015). However, most validation and comparative studies have several issues in common. 1) Validation results across studies are typically not consistent or comparable because of differences in the selection of validation data sets (i.e., time and location, and quality of field measurements) and the use of validation methodology (i.e., treatment of data quality flags, and choice of spatial and temporal aggregation). 2) Many validation studies have been conducted by algorithm developers.

* Corresponding author at: Department of Geographical Sciences, University of Maryland, 1127 LeFrak Hall, College Park, MD 20742, USA.
E-mail address: ddwang@umd.edu (D. Wang).

https://doi.org/10.1016/j.rse.2021.112639
Received 4 February 2021; Received in revised form 27 June 2021; Accepted 4 August 2021
Available online 11 August 2021

The limitations and weaknesses of the algorithms might not be fully revealed without the different perspectives of independent investigators. 3) Many efforts have been made to validate individual algorithms or products. The few comparative studies have focused mainly on data products rather than retrieval algorithms. While the assessment of data products is one way of indirectly evaluating retrieval algorithms, variation in input data quality and differences in algorithm implementation and data processing mean that the accuracy of the final data products does not always reflect the reliability of the retrieval algorithms used.

It is essential to fully understand the strengths and weaknesses of DSR retrieval algorithms, so that appropriate algorithms can be selected according to specific requirements and scenarios. More importantly, it is ideal to take advantage of various retrieval approaches by integrating multiple DSR estimation algorithms. The overarching goal of this study is to generate improved DSR estimates by synergizing existing retrieval approaches. The study consists of two major components. First, we implement and evaluate five representative DSR retrieval algorithms with consistent satellite data input, from the Moderate Resolution Imaging Spectroradiometer (MODIS) and other ancillary datasets. Second, to overcome the limitations of estimating retrievals using a single approach and to take advantage of the strengths of various algorithms, we propose an algorithm-integration framework to combine the results of multiple retrieval algorithms and to generate consistent DSR estimates with improved accuracy.

The five DSR retrieval algorithms evaluated are described in Section 2. Section 3 summarizes the field measurements, satellite data and products, and ancillary datasets. The results of validation and comparison are presented and discussed in Section 4. Section 5 concludes with the major findings.

2. Methodology

2.1. DSR retrieval algorithms

DSR is a function of atmospheric and surface attenuation and interactions of extraterrestrial solar irradiance, which varies with the Earth–Sun distance and solar elevation angle. Atmospheric radiative transfer models can forwardly compute DSR with high accuracy if the spatial distribution and optical characteristics of atmospheric constituents, such as gas molecules, particulate matter, cloud droplets, and surface reflectivity, are known (Mayer and Kylling, 2005). However, the direct use of highly complex radiative transfer codes in producing global DSR products is typically infeasible due to the high computational cost and the need for a large number of input parameters (Huang et al., 2019).

Radiative transfer computation can be simplified or approximated for deriving DSR from the reduced input of atmospheric and surface parameters (Huang et al., 2018; Xie et al., 2016). This approach constitutes a 'forward' algorithm, in the sense that it uses the forward modeling of atmospheric radiative transfer, although satellite observations may still need to be inverted for use as input parameters. Here, we evaluated one forward approach, the parameterization method.

The other category of DSR retrieval algorithms involves 'inverse' approaches, which estimate DSR from the top-of-atmosphere (TOA) data directly observed by satellite sensors (Pinker, 1995). Some inverse methods are based on atmospheric radiative transfer theory and produce DSR values via the inversion of physical models. Other inverse approaches are more statistical in nature, utilizing the empirical relationship between satellite data and DSR. Here, we evaluated two physics-based methods (look-up table (LUT) and optimization) and two statistical approaches (direct estimation and neural network).

2.1.1. Parameterization

Parameterization is the only forward approach evaluated in this study. The complex radiation transfer process within the atmosphere can be approximated with acceptable accuracy via a series of simple empirically parameterized formulae. This lays out the basic foundation of the parameterization approach, which parameterizes the radiative transfer model using simplified mathematical equations with a reduced complexity of input variables (Van Laake and Sanchez-Azofeifa, 2004). Compared to the explicit calculation of the atmospheric radiative transfer model, parameterization can significantly improve computational efficiency as well as reduce the number and complexity of input parameters (Qin et al., 2015). The specific schemes of parameterization differ in their assumptions and simplifications of the radiative transfer process as well as the choice of mathematical equations. Besides, the performance of the parameterization methods is depend on the selection and quality of input variables. Some study mainly relied on MODIS data products (Tang et al., 2017a; Tang et al., 2017b), and some combined multiple sources of datasets, such as reanalysis data and multisource satellite products (Tang et al., 2019a; Tang et al., 2016).

Here, we used the improved parameterization algorithm developed by Huang et al. (2018). This all-sky broadband parameterization scheme explicitly accounts for the interactions between the atmosphere and the surface. Compared to earlier approaches, this method better parameterizes the multiple scattering process within clouds (Huang et al., 2018). Its parameters are derived from simulated data for a range of solar angles, atmospheric profiles, and aerosol and cloud types. This parameterization approach uses several MODIS products for atmospheric and surface parameters as input; these parameters include aerosol optical depth (AOD), cloud effective radius, cloud water path, and surface broadband albedo. A full list of input variables is shown in Table 1.

2.1.2. LUT

The LUT approach is a physics-based approach that inverts the DSR from satellite observations of the TOA reflectance. The LUT-based approach assessed here is the narrowband approach for estimating the surface broadband shortwave flux (Liang et al., 2006). The LUT approach was named after the two look-up tables used to derive TOA reflectance (reflectance LUT) and surface DSR (flux LUT). The use of the LUT files, which store the pre-calculated results of atmospheric radiative transfer simulations, avoids the need for online execution of radiative transfer models for each individual retrieval. In addition to the narrowband LUT approach, the broadband DSR retrieval approach uses the TOA broadband albedo to infer atmospheric information and, thus, retrieve DSR (Pinker, 1995).

The narrowband LUT approach was originally developed for estimating the photosynthetically active radiation (PAR), the visible component of DSR, from MODIS data (Liang et al., 2006). Following a series of improvements and refinements, this approach is currently used to generate the global MODIS land surface DSR and PAR products (MCD18) (Wang et al., 2020).

The LUT approach assessed here involves two major steps. The atmospheric parameters are first obtained by matching the TOA reflectance calculated from the reflectance LUT with that observed by the satellite. In the initial version of the narrowband algorithm, surface reflectance data was retrieved from MODIS time series data using a minimal blue band reflectance approach (Liang et al., 2006). As an alternative, the surface reflectance data can be obtained directly from the existing product (Wang et al., 2020). Using the atmospheric parameters estimated in the first step and the surface reflectance information, DSR is generated in the second step by searching the flux LUT.

2.1.3. Optimization

The optimization algorithm is another physics-based inversion approach (Zhang et al., 2018). This method optimizes both the atmospheric and surface parameters in atmospheric radiative transfer modeling by minimizing a cost function that accounts for the difference between the observed and predicted TOA reflectance. DSR is then calculated from the optimized atmospheric and surface parameters. In

Table 1
List of input variables required by the five downward shortwave radiation (DSR) retrieval algorithms.

Algorithm	Input variable	Sources	Temporal resolution	Spatial resolution
Parameterization	Surface pressure	MERRA2	hourly	0.625*0.5°
	AOD	MODATML2	MODIS swath	10 km
		MERRA2	3-hourly	0.625°*0.5°
	Precipitable water	MOD07_L2	MODIS swath	5 km
		MERRA2	hourly	0.625*0.5°
	Ozone	MERRA2	hourly	0.625*0.5°
	Surface albedo	MCD43A3	daily	500 m
	Cloud phase	MODATML2	MODIS swath	5 km
	Cloud water path	MODATML2	MODIS swath	5 km
	Cloud effective radius	MODATML2	MODIS swath	5 km
LUT	TOA reflectance	MOD021KM	MODIS swath	1 km
	Surface reflectance	MCD43A3	daily	500 m
	Precipitable water	MOD07_L2	MODIS swath	5 km
		MERRA2	hourly	0.625*0.5°
	Elevation	GTOPO30	static	30’
Optimization	TOA reflectance	MOD021KM	MODIS swath	1 km
	Surface reflectance	MCD43A3	daily	500 m
	Cloud mask	MOD35_L2	MODIS swath	1 km
	Precipitable water	MOD07_L2	MODIS swath	5 km
		MERRA2	hourly	0.625*0.5°
	Elevation	GTOPO30	static	30’
Direct estimation	TOA reflectance	MOD021KM	MODIS swath	1 km
	Cloud mask	MOD35_L2	MODIS swath	1 km
	Surface albedo	MCD43A3	daily	500 m
Neural network	TOA radiance	MOD021KM	MODIS swath	1 km
	Cloud mask	MOD35_L2	MODIS swath	1 km

addition to the MODIS data, the optimization approach has been extended to generate DSR from the Visible Infrared Imaging Radiometer Suite (VIIRS) (Zhang et al., 2020b) and Advanced Baseline Imager (ABI) data (Zhang et al., 2021).

The optimization approach can be viewed as an extension of the LUT approach, in the sense that it also uses the two LUT files to derive the spectral TOA reflectance and surface DSR. The major difference is that the optimization approach can simultaneously retrieve atmospheric and surface parameters from TOA observations and take advantage of multispectral information, while the LUT method uses data from a single band.

2.1.4. Direct estimation

The direct estimation approach is one of the two statistical inversion methods assessed here. It consists of two major steps (Zhang et al., 2019). In the first step, which gives the method its name, the surface shortwave net radiation is directly estimated from the MODIS TOA spectral reflectance based on the statistical relationship between the two variables (Wang et al., 2015a; Wang et al., 2015b). DSR is then calculated from the surface shortwave net radiation and surface albedo.

The first step in estimating the surface shortwave net radiation is the core component of the direct estimation approach. Surface shortwave net radiation is the difference between the surface incident shortwave radiation and the shortwave radiation reflected by the surface, and is equal to the shortwave radiation absorbed at the surface. The shortwave radiation absorbed at the surface is highly correlated with that absorbed at the TOA (Kim and Liang, 2010; Pinker et al., 1985). Based on this relationship, the surface shortwave net radiation can be estimated from the TOA broadband reflectance (Cess and Vulis, 1989). Wang and Liang (2014b) demonstrated that the surface shortwave net radiation can also be estimated from the TOA spectral reflectance. This constitutes the basis for estimating DSR from multispectral MODIS data. This approach is currently used as the operational retrieval algorithm for generating the DSR product (Zhang et al., 2019) of the Global LAnd Surface Satellite (GLASS) products suite (Liang et al., 2021).

2.1.5. Neural network

Machine learning has recently been used to estimate DSR because of its flexibility and efficiency in modeling the nonlinearity between DSR and satellite data. Frequently used machine-learning methods include the gradient boosting regression tree (GBRT) (Wei et al., 2019), random forest (Hou et al., 2020), and neural network (Ryu et al., 2018; Takenaka et al., 2011) methods. The reliability of machine learning for estimating DSR has been demonstrated, particularly using GBRT and neural network methods (Brown et al., 2020; Hou et al., 2020; Wei et al., 2019). The theory of estimating DSR using neural network methods and the process of constructing the networks were comprehensively documented by Takenaka et al. (2011). The deep learning approach, which is able to use sophisticated architecture to approximate high complexity of the nonlinear patterns, recently found its applications in DSR estimation (Ma et al., 2020).

Here, we evaluated the neural network-based retrieval approach developed by Brown et al. (2020) for estimating DSR from MODIS TOA data. The model inputs include the TOA spectral reflectance of the seven MODIS land channels (Bands 1–7) and their viewing geometry data as well as cloud coverage information. The independent variables were normalized before training. We followed the same architecture developed by Brown et al. (2020), which includes one input layer with 11 neurons, one hidden layer with 14 neurons, and one output layer with one neuron. The original method employed sigmoid as the activation function. To expedite convergence and improve model performance, we changed it to the rectified linear unit (ReLU) activation function.

2.2. Algorithm integration

The five DSR retrieval algorithms assessed in this study have different theoretical foundations and conceptual frameworks. Each has specific strengths and limitations. It is useful to develop an algorithm-integration strategy that combines DSR estimates from multiple retrieval approaches to improve the accuracy and consistency of the final DSR results.

A range of data integration algorithms have been developed (Wang, 2012). Machine learning-based approaches have recently gained popularity in data integration; machine learning uses nonlinear models to establish the relationship between the integrated results, original estimates, and ancillary information (Zhang et al., 2020a). Here, we used the neural network algorithm to combine the results of the five DSR retrieval approaches. In addition to the DSR estimates, information on the view geometry and environmental conditions of the retrievals was used as the neural network input. The ancillary variables included solar zenith angle, view zenith angle, relative azimuth angle, cloud coverage, total column water vapor, and surface broadband albedo. A multilayer perceptron network with two hidden layers of 25 and five neurons, respectively, was used. ReLU was chosen as the activation function.

Additionally, we used a linear regression approach for algorithm integration and compared it with the machine-learning approach. Given its simplicity and efficiency, the linear regression approach has been

used to integrate many remote sensing data products (Shi and Liang, 2013; Wang and Liang, 2014a). The linear approach calculates the integrated result as the optimal linear combination of the individual retrievals. In some circumstances, the best linear predictor is also the best predictor (Gandin, 1965). In the linear approach, the integrated DSR was modeled as the weighted average of the DSR estimates from the five retrieval algorithms.

The major procedures for DSR retrieval and integration are summarized in Fig. 1. DSR is first estimated by the five inverse or forward retrieval algorithms from MODIS TOA data, atmospheric and surface products, as well as other ancillary information. The intermediate DSR estimates are then used as the input of the algorithm integration process. The integration methods, which are based on either linear regression or machine learning and trained with field measurements, generate improved estimates of DSR.

3. Data sets

Three groups of data—DSR field measurements, MODIS data and products, and ancillary data for algorithm development and uncertainty analysis—were used in this study.

3.1. Field measurement

DSR is measured by many weather stations, flux towers, or stations designated for radiation studies. The quality and consistency of the measurements varies and depends on many factors. The Baseline Surface Radiation Network (BSRN), an international measurement network, was established by the World Climate Research Programme (WCRP) in the late 1980s to provide reliable ground truth data for validating satellite-retrieved and model-simulated surface radiative fluxes, and to facilitate climatic studies on surface radiation variability (Driemel et al., 2018; Ohmura et al., 1998). At BSRN stations, a cavity radiometer or thermopile pyrheliometer is used for direct DSR measurement. A pyranometer is used to measure the total DSR, and a shaded pyranometer to measure the diffuse DSR. In addition to surface irradiance, BSRN sites typically collect surface meteorological variables and atmospheric profile information.

The BSRN stations cover a variety of latitudes, altitude, land cover, and climate zones. BSRN maintains a strict standard and delivers a consistently high-quality dataset for the entire globe. The BSRN accuracy requirement for total DSR is 5 W/m^2, and that for direct DSR is 2 W/m^2. BSRN is an ideal data source for comparing the five retrieval algorithms over various scenarios. DSR measurements for 2013, from 25 BSRN stations, were obtained (Table 2). DSR is measured at BSRN stations at very high frequencies (~1 Hz), and the averaged data for each minute are archived. We downloaded the 1-min data from these stations. The field measurements within a 30-min window of the MODIS overpass time were aggregated for comparison with the MODIS retrievals to mitigate the influence of spatial resolution mismatches and 3D cloud effects (Huang et al., 2016a).

Among the five retrieval algorithms, the parameters of the two statistical approaches needed to be tuned. The direct estimation approach was trained using simulated data, while the neural network approach required field measurements for training. To maximize the amount of in-situ data that can be used for validation and intercomparison, we used the DSR measurements from four Surface Radiation Budget (SURFRAD) stations (Augustine et al., 2005), which are not part of the 25 BSRN stations, to train the neural network (Table 3). At SURFRAD, Normal Incidence Pryheliometers are used to measure the direct DSR, and Eppley 8–48 pyranometers are used for diffuse DSR measurement. One

Table 2
Information of the Baseline Surface Radiation Network (BSRN) stations used for algorithm validation.

Site No.	Site name	Latitude	Longitude	Elevation (m)	Continent
1	GOB	−23.56	15.04	407	Africa
2	TAM	22.79	5.53	1385	
3	FUA	33.58	130.38	3	Asia
4	ISH	24.34	124.16	6	
5	XIA	39.75	116.96	32	
6	ASP	−23.80	133.89	547	Oceania
7	DAR	−12.43	130.89	30	
8	DWN	−12.42	130.89	32	
9	LAU	−45.05	169.69	350	
10	CAB	51.97	4.93	0	Europe
11	CAM	50.22	−5.32	88	
12	CAR	44.08	5.06	100	
13	CNR	42.82	−1.60	471	
14	LER	60.14	−1.18	80	
15	LIN	52.21	14.12	125	
16	PAL	48.71	2.21	156	
17	BIL	36.61	−97.52	317	North America
18	BON	40.07	−88.37	213	
19	DRA	36.63	−116.02	1007	
20	E13	36.61	−97.49	318	
21	GCR	34.25	−89.87	98	
22	PSU	40.72	−77.93	376	
23	BRB	−15.60	−47.71	1023	South America
24	PTR	−9.07	−40.32	387	
25	SMS	−29.44	−53.82	489	

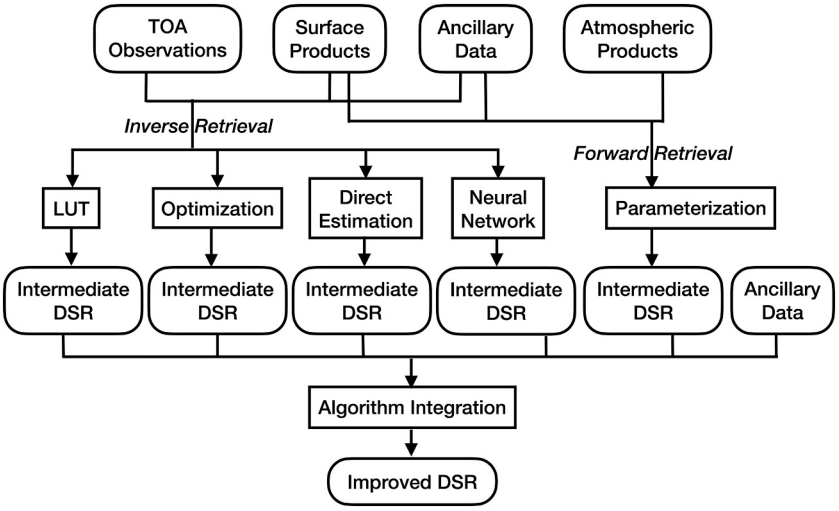

Fig. 1. Data flow of algorithm integration for improving downward shortwave radiation (DSR) estimation.

Table 3
List of the four Surface Radiation Budget (SURFRAD) stations used for training the neural network.

Site No.	Site name	Latitude	Longitude	Elevation (m)
1	FPK	48.31	−105.10	634
2	GWN	34.25	−89.87	98
3	SXF	43.73	−96.62	473
4	TBL	40.12	−105.24	1689

year data of 1-min SURFRAD measurements were downloaded.

3.2. MODIS data

We used several MODIS data products as the main satellite inputs for the DSR retrieval algorithms. Each MODIS data product has a unique Earth Science Data Type (ESTD) name, which we used here to identify the MODIS products. The MODIS sensors are onboard two satellites, named Terra and Aqua. ESDT names from the two sensors use a different prefix. For simplicity, we list only the ESDT names of the MODIS/Terra products, although data from both sensors were used in the study.

MOD021KM and MOD03 are MODIS L1B products. MOD021KM is TOA spectral reflectance data at a 1-km resolution. MOD03 is the corresponding geolocation and view geometry information. The number of MODIS observations per day varies with latitude. By combining Terra and Aqua, we achieved more than two daytime observations per day for most parts of the world. The L1B datasets contain MODIS spectral radiance data after radiometric calibration and geometric correction (Xiong et al., 2007). The L1B observational data were used as the input for all MODIS upstream high-level products. Among the five DSR retrieval algorithms, the four inversion approaches required TOA spectral reflectance data and their corresponding view geometry.

MOD35_L2, the MODIS cloud mask product, uses a variety of tests based on the MODIS solar-reflective and thermal bands to produce the cloud mask at a 1-km resolution (Ackerman et al., 1998). Optimization and direct estimation approaches select different retrieval paths according to whether clouds are present or not. This product was also used as input for the neural network approach.

MCD43A3, the MODIS albedo product, is the only gridded MODIS product we used (Schaaf et al., 2002). In its early versions, MODIS albedo values were updated every eight days. The latest Collection 6 data use a temporally weighted approach that emphasizes the contribution of the current day's observations to estimate the daily albedo. The MODIS daily albedo product was used for four of the retrieval algorithms.

MOD07_L2 is the MODIS atmosphere profile product, containing several atmospheric parameters (King et al., 2003), of which precipitable water was used as input for three of the retrieval algorithms.

MODATML2, the MODIS joint atmosphere product, combines several high-level products generated by the MODIS atmospheric team; these include aerosol (Levy et al., 2013) and cloud optical properties (Platnick et al., 2017). This combined product serves as the basis of several key inputs, including AOD, cloud effective radius, cloud water path, and cloud phase, needed by the parameterization approach.

3.3. Other data sets

Two of the DSR retrieval algorithms evaluated here require surface elevation data, for LUT selection and interpolation. These data were obtained from the GTOPO30 product. GTOPO30 is a global digital elevation model (DEM) dataset with a spatial resolution of 30 arc-seconds, developed by the United States Geological Survey (USGS). This dataset is also used in the production of the MODIS DSR product (MCD18A1).

A global reanalysis dataset, Modern-Era Retrospective Analysis for Research and Application Version 2 (MERRA2), was used. MERRA2 was developed by the NASA Global Modeling and Assimilation Office (Molod et al., 2015). Although available at a coarse spatial resolution, MERRA2 data are spatially complete. MERRA2 surface pressure and ozone concentrations were used for the parameterization approach. Total column water vapor and AOD were obtained from MERRA2 when MODIS products for those variables were not available.

Due to the similarity between the optical characteristics of snow and clouds, it is a challenge to estimate DSR over snow-covered surfaces. To assess the performance of the five algorithms over snow, snow cover data were used. Although MODIS has its own snow cover product, it is available only for clear-sky pixels and is limited by the ability of optical sensors to discriminate between snow and clouds. Here, we used all-sky Interactive Multisensor Snow and Ice Mapping System (IMS) snow map data; in this product, satellite data from various sources, including optical, passive microwave, and RADAR sensors onboard polar and geostationary satellites, are combined to generate IMS binary snow cover data at a 4-km resolution (Helfrich et al., 2007). However, IMS snow data have no coverage in the Southern Hemisphere. Another all-sky snow cover product, the Near-Real-Time SSM/I-SSMIS EASE-Grid Daily Global Ice Concentration and Snow Extent (NISE) snow map, was used when IMS data were not available. Compared to IMS, the NISE snow map has a coarser spatial resolution (25 km).

4. Results and discussion

4.1. DSR retrieval methods

4.1.1. Overall performance

We compared the DSR retrievals from the five algorithms using all available MODIS data with the field measurements of DSR. The direct estimation model was established using the simulated data, and the neural network was trained with the data from four SURFRAD stations, which are not part of the 25 BSRN sites. Thus, the ground truth data from all of the 25 BSRN sites were used to validate the five algorithms (Fig. 2). In terms of accuracy, the parameterization method produced the most accurate DSR, with an RMSE of 91.7 W/m^2 and a bias of 6.7 W/m^2; the LUT approach was the second most accurate, by ~10 W/m^2 higher in RMSE; the optimization follows, by 6 W/m^2 higher in RMSE than that of the LUT approach. The two statistical methods had the worst performance. Direct estimation produced a small number of negative DSR values (1.6%), due to the unbounded nature of linear regressions; excluding negative values improved the DSR estimates slightly, reducing their RMSE and bias by 2 W/m^2. The neural network approach produced only positive DSR values because it applies the ReLU activation function. In contrast to the two statistical methods, the remaining three approaches are all physically constrained because they are based either on offline radiative transfer models or the parameterization of radiative transfer models.

It should be noted that the five approaches generated different numbers of valid retrievals; this is because they require different sets of input variables. The availability of combinations of input data varied across methods. As expected, the optimization and neural network approaches had most valid DSR retrievals because they require only TOA spectral reflectance and cloud mask data. The LUT and direct estimation approaches produced 2% fewer retrievals because they additionally require spectral or broadband surface albedo data. The parameterization approach had the fewest valid results, i.e., it generated 22% fewer retrievals than the optimization or neural network approaches, even when invalid MODIS AOD data were replaced with MERRA2 reanalysis data. When only MODIS AOD data were used, the parameterization approach had 44% fewer valid retrievals. This is not surprising because the parameterization approach requires the most input parameters. The satellite products for several input variables, such as aerosol and cloud parameters, had many missing values.

The results were also examined by station (Table 4) and sensor (Table 5). The relative performance of the five retrieval approaches was consistent over all stations. Parameterization produced the smallest

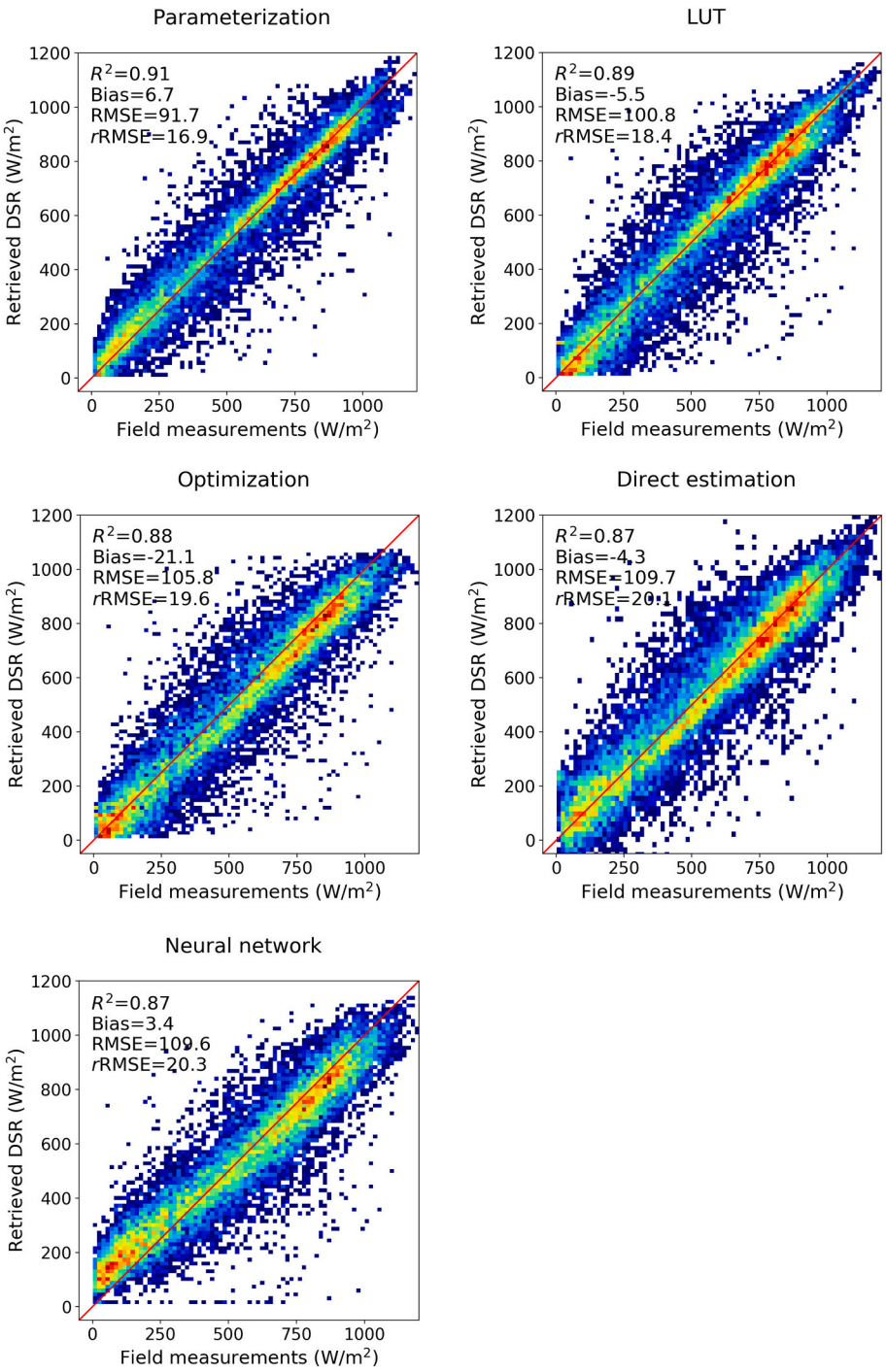

Fig. 2. Comparison of all available satellite downward shortwave radiation (DSR) data retrieved from the five algorithms with the Baseline Surface Radiation Network (BSRN) measurements. The red lines are 1:1 lines. The colors in the scatter plots represent the point density, blue = low point density, red = high point density. *r*RMSE is the relative root mean square error (RMSE). (For interpretation of the references to colour in this figure legend, the reader is referred to the web version of this article.)

errors, almost over all stations. The performance of the DSR retrieval approaches varied substantially across various stations. It is found that the accuracy of DSR estimates mainly changes with several factors such as view geometry, snow and cloud coverage. The impacts of these factors will be discussed in detail in the following sections. It is also noted that climate type plays an important role in determining the validation statistics at the station level. Sites with dynamic weather tend to be associated with lower accuracy in estimating DSR. For example, GOB, where the frequency of cloudy-sky cases is less than 5%, sees the best performance with relative RMSE as low as 5.5%. On the other hand, LER with cloudy-sky cases around 80% has the highest relative RMSE of 31.8% among all the results from parameterization. This phenomena can be attributed to two factors. All the retrieval algorithms evaluated in the study produce higher accuracy for clear-sky cases. Besides, the dynamic changes of atmospheric conditions exaggerates the 3-dimensional effect of clouds (Jiang et al., 2020) and increases uncertainties in algorithm validation.

The accuracy of the five approaches had a similar ranking across the two MODIS sensor (Table 5). Parameterization outperformed the other four approaches for both MODIS/Aqua and MODIS/Terra data. Interestingly, all the five retrieval approaches produced slightly better results for MODIS/Terra than for MODIS/Aqua. Further investigation is needed to attribute the difference to the radiometric performance of the two sensors or the diurnal variability in surface and atmospheric parameters.

Table 4
Summary of validation results for the five DSR retrieval algorithms at the 25 BSRN sites.

Site	Parameterization				LUT				Optimization				Direct estimation				Neural network			
	R^2	RMSE	Bias	*r*RMSE	R^2	RMSE	Bias	*r*RMSE	R^2	RMSE	Bias	*r*RMSE	R^2	RMSE	Bias	*r*RMSE	R^2	RMSE	Bias	*r*RMSE
GOB	0.96	42.9	9.9	5.5	0.93	52.8	22.7	6.6	0.92	55.3	−16.9	6.9	0.88	64.1	−3.9	8.0	0.89	82.4	−52.8	10.3
TAM	0.80	105.7	−65.8	11.6	0.77	103.5	−46.6	11.6	0.76	138.3	−102.2	15.4	0.75	115.6	−59.3	12.9	0.78	141.9	−108.9	15.8
FUA	0.91	87.6	13.8	17.5	0.89	96.5	18.8	19.1	0.89	96.7	−0.9	19.1	0.87	103.8	9.6	20.5	0.85	109.3	3.5	21.6
ISH	0.77	134.8	−21.3	21.5	0.78	134.2	−45.8	20.8	0.78	129.6	0.6	20.0	0.79	131.5	−8.8	20.3	0.78	126.2	−9.9	19.5
XIA	0.92	77.0	2.8	14.8	0.91	85.5	37.5	16.3	0.89	87.6	19.2	16.7	0.87	105.5	47.1	20.1	0.86	104.4	33.2	19.9
ASP	0.91	82.6	17.7	11.2	0.88	85.0	−9.9	11.6	0.88	93.5	−34.3	12.8	0.85	102.8	−35.1	14.1	0.90	79.0	12.1	10.8
DAR	0.75	116.6	19.7	17.3	0.68	122.6	−5.8	17.6	0.66	127.6	13.0	18.4	0.63	135.2	14.4	19.4	0.70	115.3	−3.3	16.6
DWN	0.77	111.8	30.3	16.5	0.65	123.0	16.1	17.6	0.62	133.1	34.6	19.0	0.61	139.4	42.2	19.9	0.64	122.0	6.3	17.4
LAU	0.86	110.7	22.9	26.3	0.82	121.3	−13.6	28.0	0.82	121.9	−35.1	28.1	0.78	130.3	−18.9	30.0	0.81	125.5	2.8	28.9
CAB	0.90	78.2	10.7	22.7	0.88	90.6	−2.6	25.7	0.87	91.2	−7.2	25.9	0.87	100.4	16.9	28.5	0.86	97.3	28.6	27.6
CAM	0.88	91.9	5.3	24.6	0.88	96.2	−1.6	24.8	0.88	96.7	−6.4	25.0	0.86	109.7	9.5	28.3	0.87	101.5	21.1	26.2
CAR	0.92	79.2	3.9	14.2	0.91	89.1	−6.8	16.1	0.91	92.5	−27.3	16.7	0.90	93.7	−7.1	16.9	0.91	88.6	−0.6	16.0
CNR	0.90	92.7	12.3	18.9	0.87	107.4	−17.6	21.3	0.86	110.3	−27.5	21.9	0.86	114.5	−8.9	22.7	0.87	100.0	−6.0	19.8
LER	0.81	90.2	4.9	31.8	0.79	98.9	10.0	37.0	0.79	97.4	0.7	36.5	0.69	118.4	16.9	44.3	0.80	105.7	43.9	39.6
LIN	0.87	91.0	4.1	27.0	0.85	106.9	−14.7	29.3	0.84	110.3	−19.3	30.3	0.84	112.6	13.2	30.9	0.80	119.0	16.9	32.7
PAL	0.88	91.8	−0.7	21.9	0.87	98.4	−14.1	22.6	0.86	99.7	−18.9	22.9	0.86	104.4	−4.2	24.0	0.85	101.9	7.7	23.4
BIL	0.92	81.2	12.3	14.2	0.90	86.9	−6.5	15.2	0.90	90.9	−25.5	15.9	0.90	91.5	−5.3	16.0	0.86	105.9	31.0	18.5
BON	0.89	91.0	−8.5	16.5	0.82	122.9	−32.8	21.7	0.84	123.4	−50.7	21.8	0.86	106.4	−23.2	18.8	0.75	139.0	−16.1	24.6
DRA	0.90	72.3	−1.0	9.4	0.84	94.1	−15.0	12.8	0.84	123.0	−82.3	16.7	0.85	97.6	−37.4	13.3	0.84	121.0	−80.8	16.4
E13	0.91	84.8	6.6	14.7	0.90	88.2	−6.2	15.4	0.90	91.0	−27.1	15.8	0.89	95.0	−11.8	16.5	0.87	103.3	31.6	18.0
GCR	0.93	78.4	2.7	14.8	0.90	94.0	−14.7	17.7	0.90	100.7	−34.9	19.0	0.89	103.1	−24.3	19.5	0.91	92.3	0.3	17.4
PSU	0.87	102.8	5.8	22.6	0.82	124.2	5.1	26.1	0.82	120.8	−12.6	25.4	0.84	119.7	−2.2	25.1	0.83	114.8	0.8	24.1
BRB	0.57	127.3	23.6	17.2	0.59	118.9	−13.2	16.0	0.57	120.9	−24.2	16.3	0.54	127.1	−19.9	17.1	0.57	120.8	−6.8	16.2
PTR	0.60	120.1	59.8	15.7	0.57	107.4	19.6	13.9	0.56	103.6	17.3	13.4	0.51	113.5	6.5	14.7	0.54	119.7	51.9	15.5
SMS	0.90	96.2	16.7	17.3	0.88	102.9	−13.4	17.8	0.87	109.6	−30.1	18.9	0.84	116.5	−17.3	20.1	0.87	106.5	−2.5	18.4

4.1.2. Validation results using identical datasets

Pixels for which some of the input data required for the parameterization approach were unavailable could be challenging for the other DSR retrieval algorithms, even though they do not directly use those input data. To ensure fair comparison, we excluded these cases from the results of the other four approaches and generated plots using identical datasets for the validation step (Fig. 3). All four approaches produced better results after the observations with missing MODIS atmospheric products had been excluded, with reductions in RMSEs ranging from 3.9 W/m^2 for optimization to 5.7 W/m^2 for direct estimation. The accuracy of the LUT approach, the second best-performing approach, improved by 5.0 W/m^2. When the same set of input data was used, the RMSE of the LUT approach was only 4.1 W/m^2 greater than that of the parameterization approach.

We then examined the impact of the availability of MODIS AOD data on the retrieval results (Figs. 4 and 5). Similarly, the availability of valid MODIS AOD data affected the DSR results of all methods, even though only parameterization requires AOD as input. Parameterization had an overall RMSE of 71.5 W/m^2 and a bias of 7.6 W/m^2 for all clear-sky cases when MERRA2 AOD data were additionally used; when using only valid MODIS AOD input, the RMSE of the parameterization approach was by more than 20 W/m^2 lower, at 47.3 W/m^2, and the bias was reduced to −1.6 W/m^2. Using the same cases for which MODIS AOD data were available resulted in a slightly higher accuracy of the LUT approach as compared to the parameterization approach.

These results clearly demonstrate that the performance of all DSR retrieval algorithms is strongly dependent on the observation conditions. All five methods tended to estimate DSR with higher accuracy under favorable atmospheric conditions, such as when MODIS aerosol parameters and cloud optical and microphysical data were available.

4.1.3. Impacts of clouds

To further evaluate the impacts of surface and atmospheric conditions on DSR retrievals, we analyzed the DSR results in terms of cloud presence and phase. We used the MODIS cloud phase product to divide the overall results into three categories: no clouds, water clouds, and ice clouds. The validation results of the five algorithms under the three different cloud conditions are summarized in Table 6.

Similar to the situation achieved disregarding cloud cover, the parameterization approach outperformed the other four approaches under all three cloud conditions, except for one scenario: for clear-sky pixels, the LUT RMSE was marginally smaller than that of the parameterization approach. All five approaches performed relatively well under clear-sky conditions. The RMSE ranged from 71.3 W/m^2 (or relative RMSE of 9.3%) of the LUT approach to 91.8 W/m^2 (12.1%) of the neural network approach. The presence of clouds significantly reduced the accuracy of the DSR estimates for all five algorithms. The lowest RMSE obtained for cloudy-sky cases was 105.7 W/m^2 (for ice clouds), using the parameterization approach. This was 34.2 W/m^2 greater than the RMSE achieved for clear-sky cases using the parameterization approach. However, the relative error was more than three times greater than that for clear-sky cases because DSR is lower when clouds are present. The estimation accuracy was similar for water and ice cloud pixels. Among the five algorithms, direct estimation produced the lowest accuracy for cloudy-sky cases, with RMSEs of 129.2 W/m^2 (32.1%) and 120.5 W/m^2 (32.9%) for water cloud and ice cloud pixels, respectively.

The challenges in estimating DSR under cloudy-sky conditions are associated with several factors. Clouds have various thermodynamic phases and complex microphysical characteristics, which lead to variability in cloud optical properties (Letu et al., 2020). DSR retrieval methods have simplified assumptions on cloud vertical structure, which typically neglect the effects of multilayer clouds (Wang et al., 2016). In addition to inhomogeneous vertical profile, horizontal distribution of clouds shows substantial spatial heterogeneity too. It results in the 3-dimensional effect of clouds in validating satellite DSR retrievals with ground measurements of DSR (Huang et al., 2016a).

Table 5
Summary of the validation results of the five DSR retrieval algorithms using MODIS/Aqua and MODIS/Terra data.

Algorithm	MODIS/Aqua				MODIS/Terra			
	R^2	RMSE	Bias	*r*RMSE	R^2	RMSE	Bias	*r*RMSE
Parameterization	0.90	95.3	3.4	17.3	0.92	89.0	9.0	16.6
LUT	0.89	101.6	−5.5	18.4	0.89	99.6	−5.1	18.5
Optimization	0.88	107.7	−24.3	19.5	0.88	103.9	−19.1	19.3
Direct estimation	0.86	113.8	−5.3	20.6	0.88	105.8	−2.7	19.6
Neural network	0.87	110.9	0.9	20.1	0.87	107.6	2.4	20.0

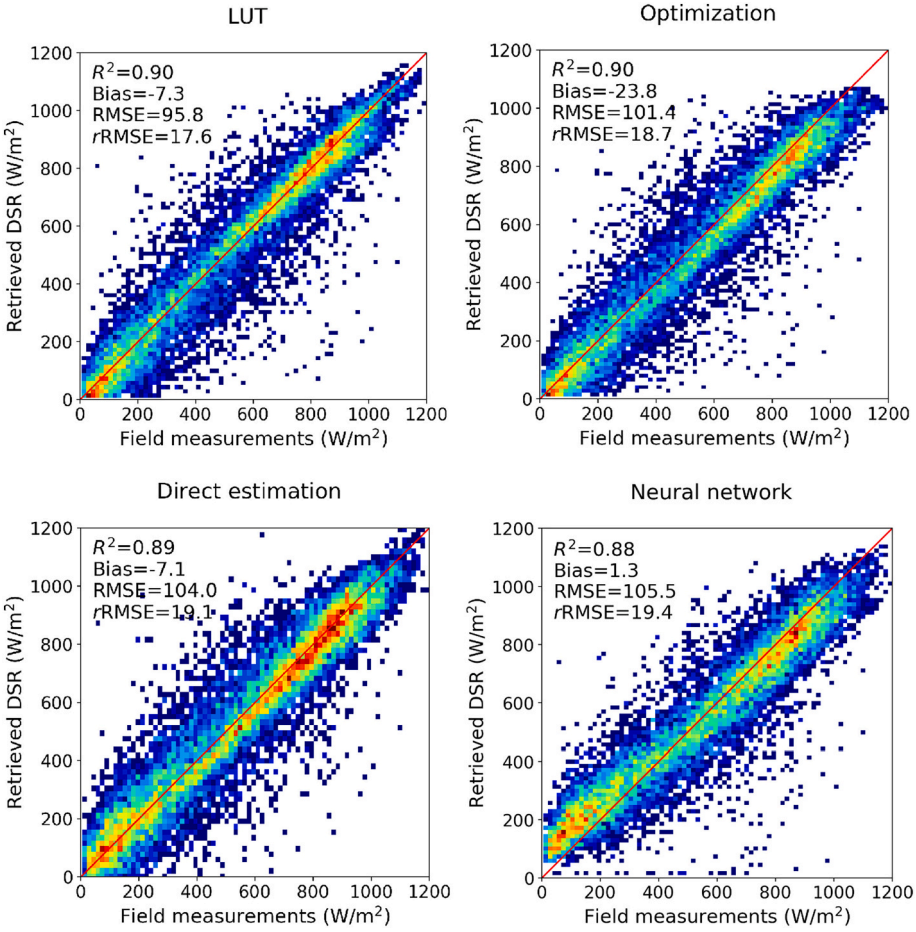

Fig. 3. Comparison of the satellite downward shortwave radiation (DSR) retrieved from the look-up table (LUT), optimization, direct estimation, and neural network approaches with the identical set of Baseline Surface Radiation Network (BSRN) measurements as parameterization.

4.1.4. Impacts of snow

Snow was a major factor affecting the performance of all DSR retrieval algorithms. All five approaches evaluated here showed a significantly poorer performance over snow-covered cases (Table 7). As before, the parameterization method produced the highest accuracy for snow-covered cases, with an RMSE of 81.4 W/m^2 or a relative RMSE of 22.6%. The direct estimation approach also produced accurate results for bright-surface cases, with an RMSE 12.4 W/m^2 greater than that of the parameterization approach. As a result, the reduction in accuracy caused by snow was smaller for the parameterization and direct estimation approaches than for the other approaches. When the surface was covered by snow, the increase in the relative RMSE was 7–8% for the parameterization and direct estimation approaches, 14–15% for the optimization and LUT approaches, and 18% for the neural network approach.

The cloud microphysical and optical products needed as input for the parameterization approach use different strategies and band combinations to handle the reduced contrast between clouds and snow in the visible channels (Platnick et al., 2017). Thus, the parameterization approach could achieve a high accuracy even when snow was present. Our evaluation reveals that the statistical models used in the direct estimation approach can handle snow cases relatively well by combining various types of multispectral information. The neural network approach produced the worst results over snow-covered cases. Further algorithm development, with additional training data over snow-covered pixels, is needed to improve the performance of the neural network approach.

4.1.5. Angular dependency of retrieval errors

The validation results were analyzed in terms of view geometry to examine the dependency of DSR retrieval accuracy on solar zenith angles, view zenith angles, and relative azimuth angles. For all five methods, the absolute RMSE values decreased with the solar zenith angle (Fig. 6). The relative RMSE increased substantially with the solar

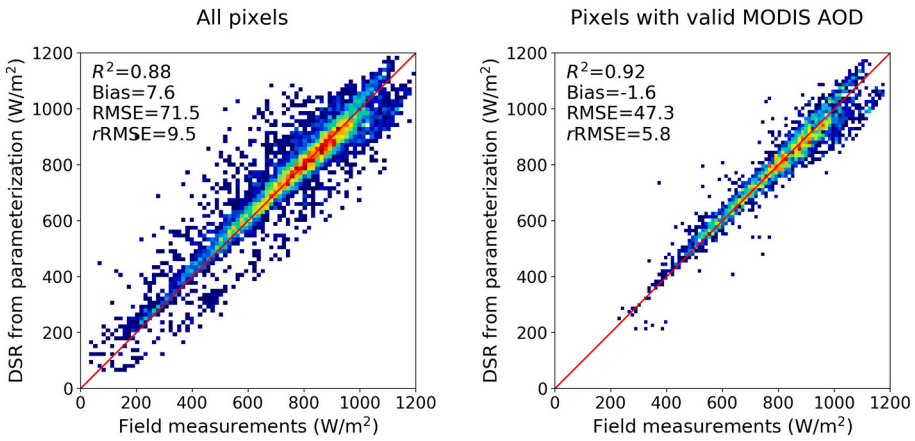

Fig. 4. Validation of clear-sky downward shortwave radiation (DSR) estimated from the parameterization approach using a) MODIS aerosol optical depth (AOD) or MERRA2 AOD and b) only MODIS AOD.

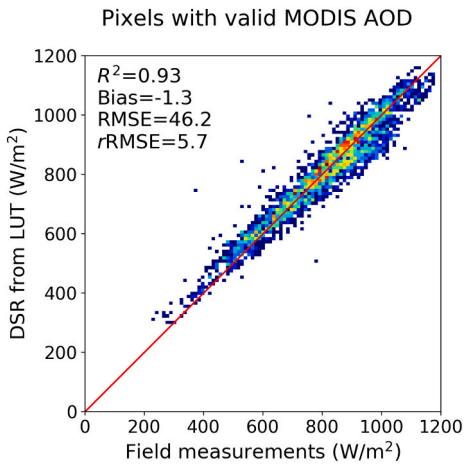

Fig. 5. Validation of clear-sky downward shortwave radiation (DSR) estimated from the look-up table (LUT) approach for the same set of pixels as in Fig. 4b (where MODIS aerosol optical depth (AOD) data are available).

zenith angle, especially above 45°, because DSR decreases with the solar zenith angle. These trends were valid for both clear-sky and cloudy-sky cases. These results reveal the challenges of obtaining relatively accurate DSR estimates when the solar zenith angle is large. There are several reasons for this difficulty. First, a larger solar zenith angle is indicative of cold seasons with a greater chance of a snow cover. Second, the length of the light-scattering path increases with the solar zenith angle. Third, a large solar zenith angle increases the uncertainty in modeling the atmospheric heterogeneity under the parallel-plane assumption and the anisotropy of the surface reflectance. Fourth, the effect of the Earth's curvature increases with the solar zenith angle.

The changes in the relative RMSE obtained using the view zenith angle were substantially smaller than those obtained using the solar zenith angle (Fig. 7). The clear-sky and cloudy-sky conditions showed distinct patterns of angular dependency. The relative RMSE changed little (within 2%) in the clear-sky results, and the patterns were not monotonic. The relative errors for estimating the cloudy-sky DSR did not change as much with the view zenith angle as with the solar zenith angle; this increase was particularly pronounced using the parametrization approach.

The dependency of the errors on the relative azimuth angle also differed between clear-sky and cloudy-sky conditions (Fig. 8). For clear-sky cases, hardly any of the trends were monotonic. For cloudy-sky cases, observations from the principal plane and the perpendicular plane produced different levels of accuracy: data from the perpendicular plane resulted in less accurate DSR estimates, potentially due to uncertainties in modeling the anisotropy of cloud reflectivity for various cloud phases (Ehrlich et al., 2008).

Table 6
Summary of the validation results of the five algorithms for three cloud scenarios (cloud-free, water clouds, and ice clouds).

Algorithm	Cloud phase	R^2	RMSE (W/m^2)	Bias (W/m^2)	*r*RMSE (%)
Parameterization	Cloud-free	0.881	71.5	7.6	9.5
	Water clouds	0.764	109.5	−15.0	32.1
	Ice clouds	0.830	105.7	35.9	32.9
LUT	Cloud-free	0.880	71.3	2.2	9.4
	Water clouds	0.746	117.1	−17.0	34.4
	Ice clouds	0.790	112.8	−16.5	35.1
Optimization	Cloud-free	0.866	80.1	−26.2	10.6
	Water clouds	0.742	119.1	−14.1	34.9
	Ice clouds	0.788	113.5	−10.8	35.3
Direct estimation	Cloud-free	0.871	76.0	−11.4	10.1
	Water clouds	0.718	129.2	−19.7	37.9
	Ice clouds	0.777	120.5	21.3	37.5
Neural network	Cloud-free	0.817	91.8	−25.4	12.1
	Water clouds	0.742	118.2	34.9	34.7
	Ice clouds	0.775	116.1	16.0	36.2

4.2. Algorithm Integration results

4.2.1. Overall results

The two algorithm-integration approaches presented here—linear regression and machine learning—are both data-driven methods: the model parameters are trained using actual measurement data. Their performance should be evaluated using a dataset that is independent of the training data. To assess the impact of the amount of training data on the integration results, we used various portions (up to 60%) of the total dataset to train the two models and tested the results using the remaining data. The errors of both approaches initially declined with an increasing amount of training data (Fig. 9). Their accuracy then plateaued and changed little with a further increase in training data. It is

Table 7
Summary of the validation results of the five algorithms for snow-covered and snow-free cases.

Algorithm	Snow-covered				Snow-free			
	R^2	RMSE (W/m^2)	Bias (W/m^2)	*r*RMSE (%)	R^2	RMSE (W/m^2)	Bias (W/m^2)	*r*RMSE (%)
Parameterization	0.900	81.4	15.1	22.6	0.914	90.5	5.1	16.6
LUT	0.811	116.3	−18.1	32.3	0.911	93.0	−6.9	17.1
Optimization	0.813	114.9	−40.8	31.9	0.904	97.7	−20.2	17.9
Direct estimation	0.874	93.8	−31.0	26.0	0.891	102.8	−7.2	18.9
Neural network	0.708	134.0	−12.3	37.2	0.892	103.2	2.2	18.9

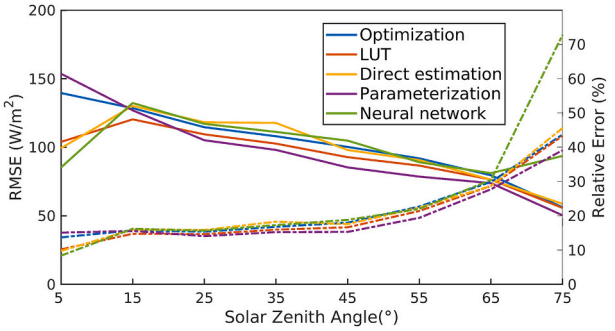

Fig. 6. Changes of estimation errors for downward shortwave radiation (DSR) with the solar zenith angle. Absolute errors are shown in solid lines and relative errors are shown in dashed lines.

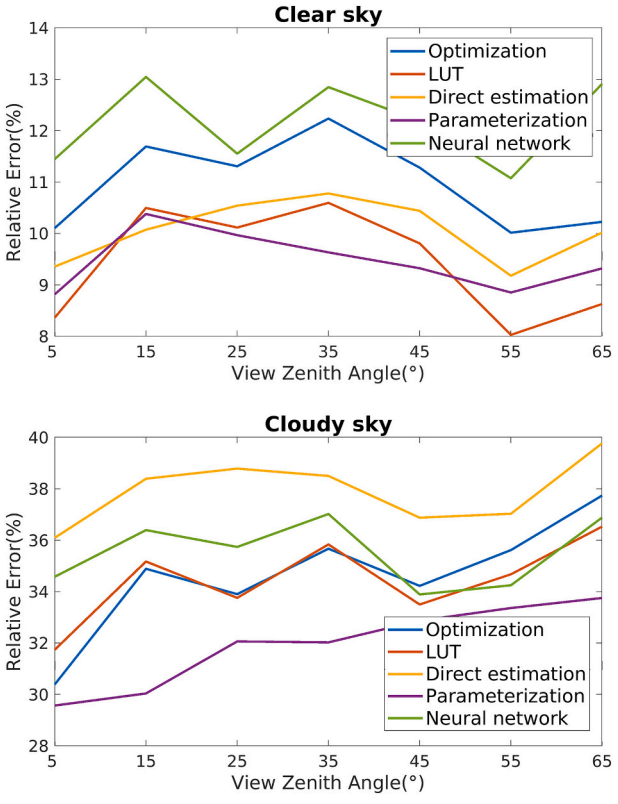

Fig. 7. Changes in estimation errors for downward shortwave radiation (DSR) with the view zenith angle.

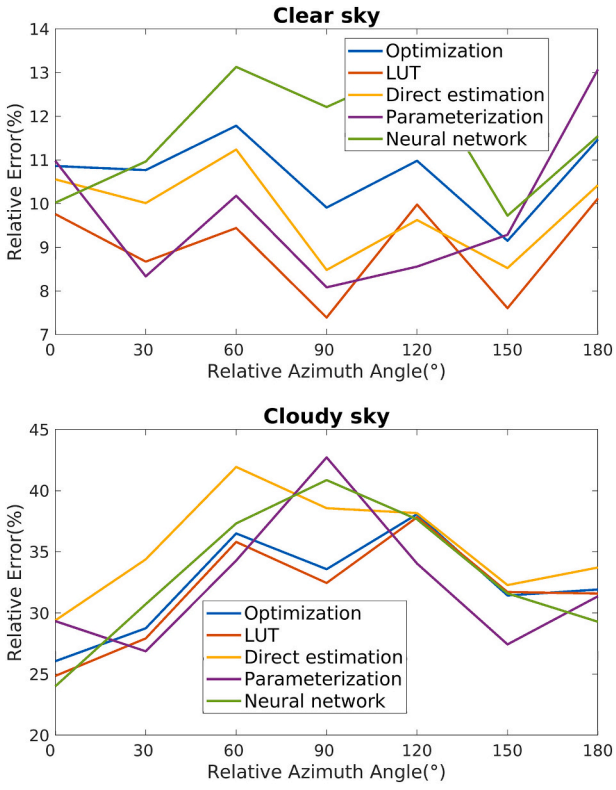

Fig. 8. Changes in estimation errors for downward shortwave radiation (DSR) with the relative azimuth angle.

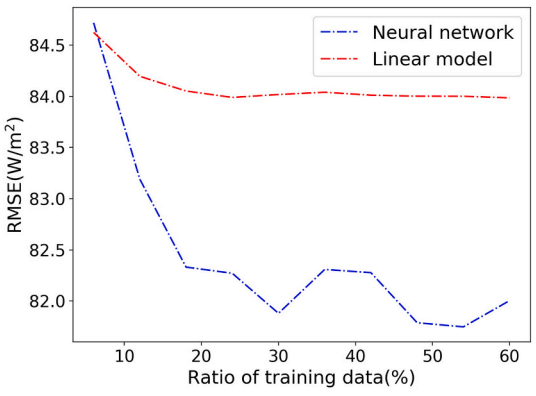

Fig. 9. Changes in the root mean square error (RMSE) of two algorithm-integration methods with the ratio of training data to total data.

not surprising that the linear model plateaued faster than the machine-learning-based approach because the former has fewer free parameters and requires less data for training. The neural network-based approach generally produced more accurate integration results (by ~2 W/m^2) than the linear regression-based integration approach. This is because the machine-learning approach can model more complex relationships between the retrieved DSR and the observed values. The use of ancillary

information as additional input to the machine-learning-based approach enables to determine the specific combination of DSR values most suited to specific scenarios.

To quantitatively evaluate the benefit of integrating multiple DSR estimates, we fixed the amount of training data to 60% of the total data and compared the integrated results with the original DSR values retrieved using the individual approaches. The DSR estimates from the best-performing retrieval algorithm (parameterization) and the results obtained using the two integration methods (Fig. 10) reveal that both integration methods significantly improved the accuracy of DSR estimation. Compared with the best retrieval algorithm, the linear regression-based method reduced the RMSE by 9 W/m^2, while the machine-learning approach reduced this value by 11 W/m^2. The two data-driven integration approaches also reduced the DSR estimation bias: linear regression and machine learning produced biases of −1.6 W/m^2 and 0.9 W/m^2, respectively.

For the demonstration in the spatial domain, the five DSR retrieval methods and the machine learning based integration approach were applied to one MODIS/Terra swath (Fig. 11). Ocean pixels were masked because the DSR retrieval algorithms evaluated here were developed for estimating land DSR. The five retrieval approaches generated DSR maps with similar spatial patterns, which were largely dominated by mesoscale clouds. It should be noted that the map from the parameterization approach contained a large number of filling values (15.8%) because of the invalid input data. The proposed integration approach requires all input parameters to be valid. As a result, filling pixels also occurred in the map of the integrated DSR.

4.2.2. *Impacts of the DSR input used in algorithm integration*

Using the DSR estimates from the five retrieval algorithms, the machine learning-based integration approach reduced RMSE of estimating DSR to 82.0 W/m^2, from 93.0 W/m^2 of the best-performing individual retrieval approach (Fig. 10). Here, we evaluated how the selection of the input data affects the integration results. Combining the two best retrieval algorithms (LUT and parameterization) achieved similar results to those obtained by integrating all five retrieval methods (Fig. 12). Combining other pairs of retrieval methods produced varied results (Fig. 13). Although the LUT and parameterization approaches produced DSR estimates with similar accuracy, the integration results using each approach were quite distinctive. The integration approach using parameterization generally produced much more accurate DSR estimates than that using the LUT approach. The worst case for including the parameterization approach had an RMSE of 85.4 W/m^2, which was by 4.7 W/m^2 lower than the best case without using the parameterization approach.

The differences in accuracy achieved by combining two approaches are likely caused by factors other than the accuracy of the individual retrieval algorithms being combined. The DSR estimation errors of the five retrieval methods were positively correlated (Fig. 14). Generally, the DSR estimation errors of the four inverse approaches were more strongly correlated than those of the other approaches. Among the four inverse approaches, the results of the neural network approach were less correlated with the results of the other three approaches. It is not surprising that the optimization and LUT approaches generated highly correlated results. The correlation coefficient between their errors was as large as 0.92 because the two approaches share similar physical foundations and use the same offline radiative transfer simulation data. The correlation coefficient between the direct estimation approach and the optimization approach was also high (0.81). The results of the forward parameterization approach were less correlated with those of the other four inversion approaches than with those between any two inversion approaches. As a result, integrating forward parameterization and an inverse approach produced better results than integrating two inversion approaches. This even produced results comparable to those obtained by integrating all five approaches.

5. Conclusions

DSR is fundamental to the Earth's radiation balance and essential in many applications. It can be estimated from satellite data using several types of retrieval approaches. Many efforts have been devoted to algorithm development, product generation, and validation. Although studies comparing multiple products are not uncommon, product comparison cannot replace the comparison of retrieval algorithms because data product quality depends not only on algorithm performance, but also on the quality of the implementation and the reliability of the input data sources. Unfortunately, few existing studies have focused on comparing retrieval approaches and understanding their strengths and limitations and scenarios in which they are most suitable.

To fill the gap, this study developed a controlled framework to evaluate five representative DSR retrieval algorithms using the consistent data as input to provide comprehensive evaluation of these retrieval methods. Based on the algorithm assessment, we presented a novel algorithm-integration approach that combines the results of the five DSR retrieval algorithms to improve the accuracy and consistency of DSR estimates.

Among the five approaches evaluated in this study, the forward parameterization approach outperformed the other four inversion approaches. Because of its efficiency and accuracy, the parameterization approach has been applied to generate global long-term data products (Tang et al., 2021; Tang et al., 2019b). Nevertheless, parameterization has its limitations. It requires the most input parameters and generates

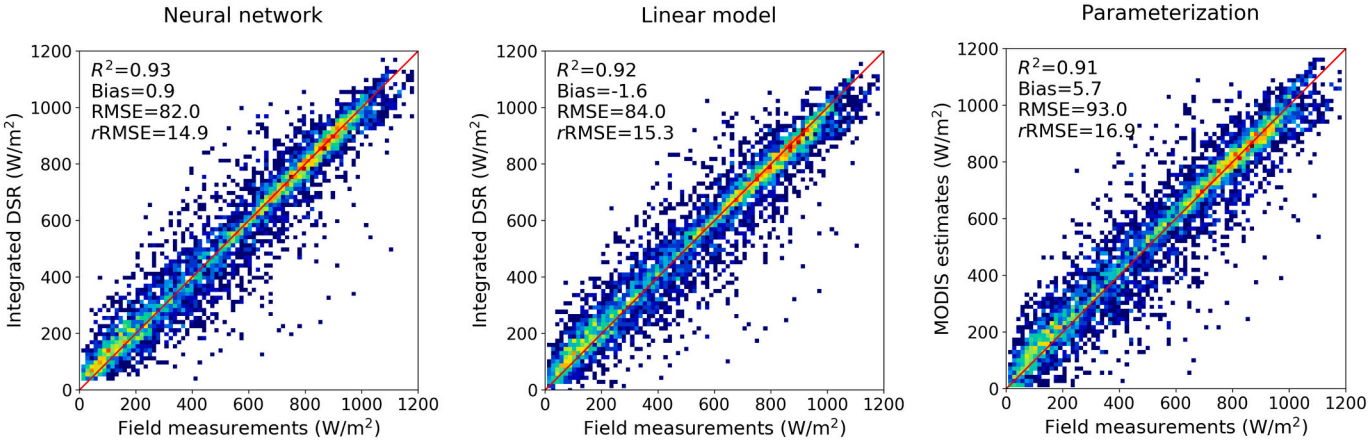

Fig. 10. Results of algorithm integration using the neural network approach and the linear regression approach. For comparison, the downward shortwave radiation (DSR) estimated from the best performance retrieval approach (parameterization) validated with the same data set is also shown.

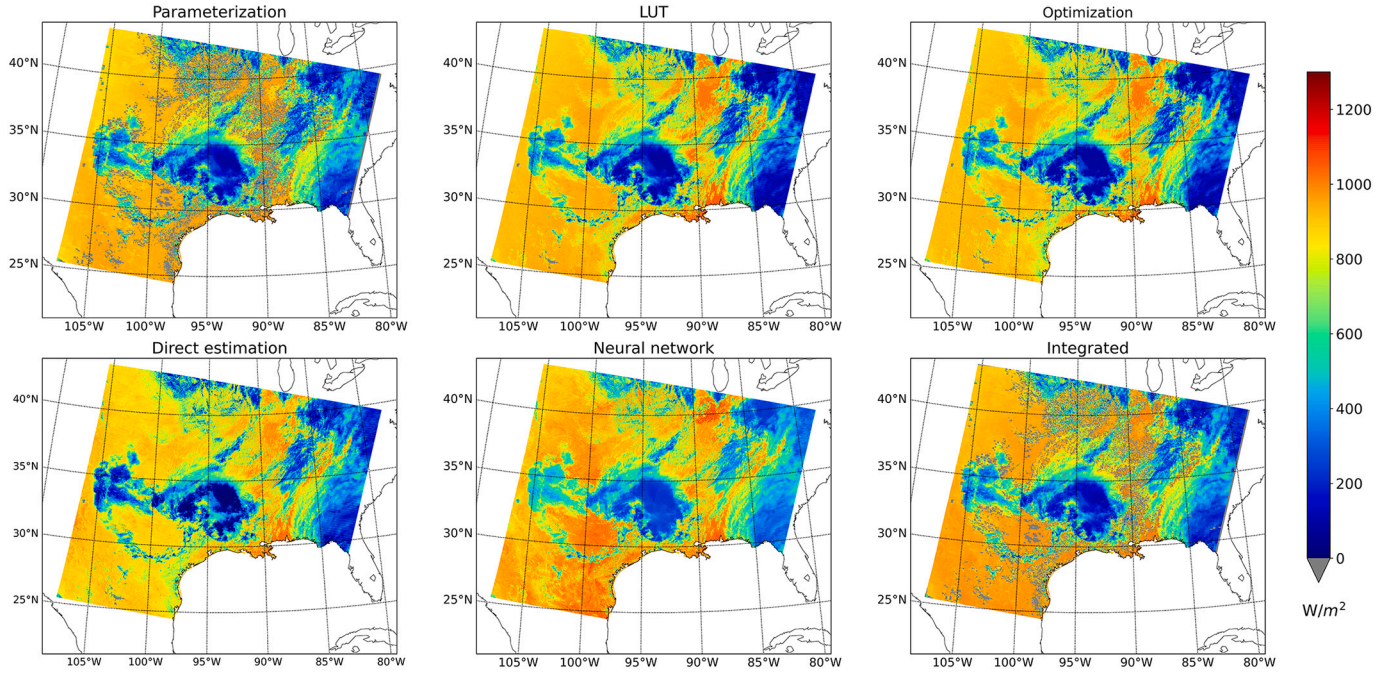

Fig. 11. DSR maps generated from the five retrieval algorithms and the algorithm integration method using the MODIS/Terra swath obtained on June 6, 2013, 17:05UTC.

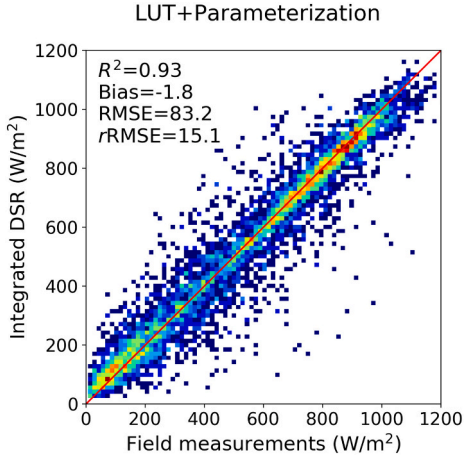

Fig. 12. Algorithm integration results of combing the look-up table (LUT) and parameterization approaches.

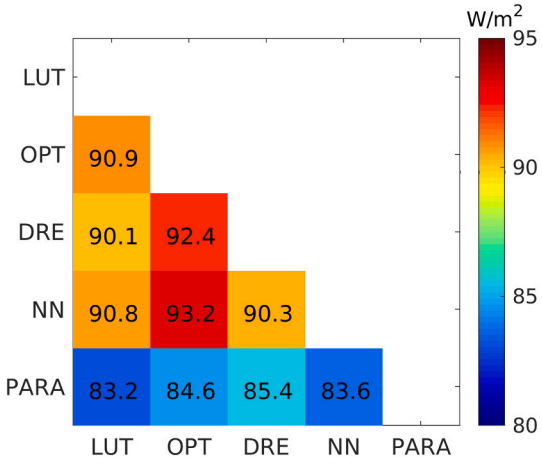

Fig. 13. Root mean square errors (RMSE) of algorithm integration using two downward shortwave radiation (DSR) retrieval algorithms.

the fewest valid retrievals. In fact, the four inversion methods all showed a better performance when only common pixels were used for validation. When an identical validation dataset was used, the RMSE of the LUT approach was only 4 W/m^2 greater than that of the parameterization approach.

The performance of the parameterization approach heavily depends on the quality of input atmospheric parameters, including aerosol and cloud optical variables. Through the continuous development and refinement of several decades, the MODIS atmospheric products are highly mature and have achieved high accuracy. The reliable input data are the pillar that the superior performance of parameterization is based on. When high quality atmospheric products are unavailable, the concepts of forward and inverse approaches can be used in a combined way. The key atmospheric parameters such as cloud optical and microphysical variables are first inversely retrieved from satellite observations and then used in the forward method to generate DSR estimates (Letu et al., 2020).

The performance of the five approaches varied with surface and atmospheric conditions. All of the approaches estimated DSR with larger uncertainty for cloudy-sky or snow-covered cases. The parameterization approach was the most reliable for almost all scenarios. After the parameterization approach, the LUT approach had the most accurate DSR estimates for clear-sky cases, and direct estimation had the best performance for snow-covered conditions (Table 8).

Our analysis reveals that algorithm integration efficiently reduces DSR estimation errors by taking advantage of multiple retrieval approaches. Even the simple linear regression-based integration model substantially improved the accuracy of the DSR estimation. The integration approach based on the neural network slightly outperformed the linear approach. By combining the results from all five retrieval approaches, the neural network approach reduced the DSR estimation error to 82.0 W/m^2 (14.9%) from 93.0 W/m^2 (16.9%) for the best-performing retrieval approach. Integration of two algorithms (a forward and an inversion approach) reduced the RMSE by 8–10 W/m^2. The

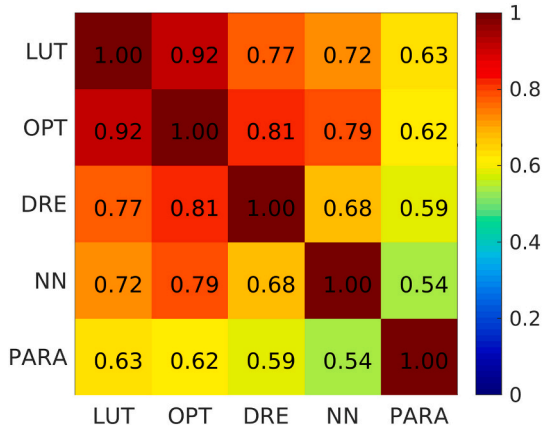

Fig. 14. Correlation coefficients of the estimation errors for the downward shortwave radiation (DSR) from the five retrieval approaches.

Table 8
Strengths and limitations of the five downward shortwave radiation (DSR) retrieval algorithms evaluated.

Method	Strength	Limitation
Parameterization	Highly accurate	Rigorous requirements for input data, in terms of the amount of variables and the accuracy of surface and atmospheric parameters
LUT	Accurate; Atmospheric parameters not required	Limited spectral information used; Not reliable for snow-covered surfaces
Optimization	Atmospheric and surface parameters not required	Computationally slow; Accuracy dependent on selection of cost function
Direct estimation	Accurate over snow-covered surfaces; Atmospheric parameters not required	Overall moderate accuracy
Neural network	Atmospheric and surface parameters not required	Accuracy dependent on quality and quantity of training data

inclusion of data from additional inversion approaches only marginally improved the integration results because the DSR estimation errors from the four inversion approaches were highly correlated.

This study identifies limitations and weaknesses of the five representative DSR retrieval approaches. Continuous algorithm development is needed to further improve the performance of individual retrieval algorithms. Future efforts should also be devoted to algorithm-integration studies that leverage the advantages of multiple retrieval algorithms. Algorithm integration is a promising way to obtain DSR estimates that are superior to estimates from any individual retrieval algorithm. This study demonstrates a framework for algorithm integration using instantaneous DSR values. The incorporation of multi-source satellite data, especially geostationary data, is of vital importance for monitoring the diurnal DSR variability. Future studies may focus on more complex data integration methods that can handle heterogeneous data sources, mismatched temporal spatial resolution and coverage, and missing and inconsistent data.

It should be noted that the evaluation results presented in the study are based on specific implementation of the retrieval algorithms. The performance of each type of DSR retrieval approaches can also be associated with other factors, such as selection of the specific algorithm, choice of radiative transfer models, configuration of model parameters, representativeness of training datasets, as well as quality of key input parameters.

Author credit statement

D. Wang conceived the research. D. Wang and R. Li processed the data. D. Wang, S. Liang, R. Li and A. Jia performed the interpretation of the results. D. Wang led the writing of the manuscript. All authors contributed to the manuscript revision.

Declaration of Competing Interest

The authors declare that they have no known competing financial interests or personal relationships that could have appeared to influence the work reported in this paper.

Acknowledgments

This study is supported by NASA (Grant ID: 80NSSC18K0620). We thank the BSRN and SURFRAD science teams for making their measurement data available.

References

Ackerman, S.A., Strabala, K.I., Menzel, W.P., Frey, R.A., Moeller, C.C., Gumley, L.E., 1998. Discriminating clear sky from clouds with MODIS. J. Geophys. Res.-Atmos. 103, 32141–32157.
Augustine, J.A., Hodges, G.B., Cornwall, C.R., Michalsky, J.J., Medina, C.I., 2005. An update on SURFRAD - The GCOS Surface Radiation budget network for the continental United States. J. Atmos. Ocean. Technol. 22, 1460–1472.
Berbery, E.H., Mitchell, K.E., Benjamin, S., Smirnova, T., Ritchie, H., Hogue, R., Radeva, E., 1999. Assessment of land-surface energy budgets from regional and global models. J. Geophys. Res.-Atmos. 104, 19329–19348.
Brown, M.G.L., Skakun, S., He, T., Liang, S.L., 2020. Intercomparison of Machine-Learning Methods for Estimating Surface Shortwave and Photosynthetically Active Radiation. Remote Sens. 12.
Cess, R.D., Vulis, I.L., 1989. Inferring Surface Solar Absorption from Broadband Satellite Measurements. J. Clim. 2, 974–985.
de Wit, A.J.W., Boogaard, H.L., van Diepen, C.A., 2005. Spatial resolution of precipitation and radiation: The effect on regional crop yield forecasts. Agric. For. Meteorol. 135, 156–168.
Driemel, A., Augustine, J., Behrens, K., Colle, S., Cox, C., Cuevas-Agullo, E., Denn, F.M., Duprat, T., Fukuda, M., Grobe, H., Haeffelin, M., Hodges, G., Hyett, N., Ijima, O., Kallis, A., Knap, W., Kustov, V., Long, C.N., Longenecker, D., Lupi, A., Maturilli, M., Mimouni, M., Ntsangwane, L., Ogihara, H., Olano, X., Olefs, M., Omori, M., Passamani, L., Pereira, E.B., Schmithusen, H., Schumacher, S., Sieger, R., Tamlyn, J., Vogt, R., Vuilleumier, L., Xia, X.G., Ohmura, A., Konig-Langlo, G., 2018. Baseline Surface Radiation Network (BSRN): structure and data description (1992-2017). Earth System Science Data 10, 1491–1501.
Ehrlich, A., Bierwirth, E., Wendisch, M., Gayet, J.F., Mioche, G., Lampert, A., Heintzenberg, J., 2008. Cloud phase identification of Arctic boundary-layer clouds from airborne spectral reflection measurements: test of three approaches. Atmos. Chem. Phys. 8, 7493–7505.
Fritz, S., Rao, P.K., Weinstein, M., 1964. Satellite measurements of reflected solar energy and the energy received at the ground. J. Atmos. Sci. 21, 141–151.
Gandin, L.S., 1965. Objective analysis of meteorological fields. Israel Program for Scientific Translations, Jerusalem.
Helfrich, S.R., McNamara, D., Ramsay, B.H., Baldwin, T., Kasheta, T., 2007. Enhancements to, and forthcoming developments in the Interactive Multisensor Snow and Ice Mapping System (IMS). Hydrol. Process. 21, 1576–1586.
Hou, N., Zhang, X.T., Zhang, W.Y., Wei, Y., Jia, K., Yao, Y.J., Jiang, B., Cheng, J., 2020. Estimation of Surface Downward Shortwave Radiation over China from Himawari-8 AHI Data Based on Random Forest. Remote Sens. *12*.
Huang, G.H., Li, X., Huang, C.L., Liu, S.M., Ma, Y.F., Chen, H., 2016a. Representativeness errors of point-scale ground-based solar radiation measurements in the validation of remote sensing products. Remote Sens. Environ. 181, 198–206.
Huang, J.P., Yu, H.P., Guan, X.D., Wang, G.Y., Guo, R.X., 2016b. Accelerated dryland expansion under climate change. Nat. Clim. Chang. 6, 166−+.
Huang, G., Liang, S., Lu, N., Ma, M., Wang, D., 2018. Toward a Broadband Parameterization Scheme for Estimating Surface Solar Irradiance: Development and Preliminary Results on MODIS Products. J. Geophys. Res.-Atmos. 123, 12180–12193.
Huang, G.H., Li, Z.Q., Li, X., Liang, S.L., Yang, K., Wang, D.D., Zhang, Y., 2019. Estimating surface solar irradiance from satellites: Past, present, and future perspectives. Remote Sens. Environ. 233.
Jiang, H., Lu, N., Huang, G.H., Yao, L., Qin, J., Liu, H.Z., 2020. Spatial scale effects on retrieval accuracy of surface solar radiation using satellite data. Appl. Energy 270.
Kim, H.Y., Liang, S., 2010. Development of a hybrid method for estimating land surface shortwave net radiation from MODIS data. Remote Sens. Environ. 114, 2393–2402.
King, M.D., Menzel, W.P., Kaufman, Y.J., Tanre, D., Gao, B.C., Platnick, S., Ackerman, S. A., Remer, L.A., Pincus, R., Hubanks, P.A., 2003. Cloud and aerosol properties, precipitable water, and profiles of temperature and water vapor from MODIS. IEEE Trans. Geosci. Remote Sens. 41, 442–458.

Letu, H.S., Yang, K., Nakajima, T.Y., Ishimoto, H., Nagao, T.M., Riedi, J., Baran, A.J., Ma, R., Wang, T.X., Shang, H.Z., Khatri, P., Chen, L.F., Shi, C.X., Shi, J.C., 2020. High-resolution retrieval of cloud microphysical properties and surface solar radiation using Himawari-8/AHI next-generation geostationary satellite. Remote Sens. Environ. 239.

Levy, R.C., Mattoo, S., Munchak, L.A., Remer, L.A., Sayer, A.M., Patadia, F., Hsu, N.C., 2013. The Collection 6 MODIS aerosol products over land and ocean. Atmosph. Meas. Techniq. 6, 2989–3034.

Liang, S., Zheng, T., Liu, R., Fang, H., Tsay, S.C., Running, S., 2006. Estimation of incident photosynthetically active radiation from Moderate Resolution Imaging Spectrometer data. J. Geophys. Res.-Atmos. 111.

Liang, S.L., Wang, D.D., He, T., Yu, Y.Y., 2019. Remote sensing of earth's energy budget: synthesis and review. Int. J. Digital Earth 12, 737–780.

Liang, S., Cheng, J., Jia, K., Jiang, B., Liu, Q., Xiao, Z., Yao, Y., Yuan, W., Zhang, X., Zhao, X., Zhou, J., 2021. The Global Land Surface Satellite (GLASS) product suite. Bull. Am. Meteorol. Soc. 102, E323–E337.

Ma, R., Letu, H.S., Yang, K., Wang, T.X., Shi, C., Xu, J., Shi, J.C., Shi, C.X., Chen, L.F., 2020. Estimation of Surface Shortwave Radiation From Himawari-8 Satellite Data Based on a Combination of Radiative Transfer and Deep Neural Network. IEEE Trans. Geosci. Remote Sens. 58, 5304–5316.

Mayer, B., Kylling, A., 2005. Technical note: The libRadtran software package for radiative transfer calculations - description and examples of use. Atmos. Chem. Phys. 5, 1855–1877.

Mellit, A., Kalogirou, S.A., 2008. Artificial intelligence techniques for photovoltaic applications: A review. Prog. Energy Combust. Sci. 34, 574–632.

Molod, A., Takacs, L., Suarez, M., Bacmeister, J., 2015. Development of the GEOS-5 atmospheric general circulation model: evolution from MERRA to MERRA2. Geosci. Model Dev. 8, 1339–1356.

Nemani, R.R., Keeling, C.D., Hashimoto, H., Jolly, W.M., Piper, S.C., Tucker, C.J., Myneni, R.B., Running, S.W., 2003. Climate-driven increases in global terrestrial net primary production from 1982 to 1999. Science 300, 1560–1563.

Ohmura, A., Dutton, E.G., Forgan, B., Frohlich, C., Gilgen, H., Hegner, H., Heimo, A., Konig-Langlo, G., McArthur, B., Muller, G., Philipona, R., Pinker, R., Whitlock, C.H., Dehne, K., Wild, M., 1998. Baseline Surface Radiation Network (BSRN/WCRP): New precision radiometry for climate research. Bull. Am. Meteorol. Soc. 79, 2115–2136.

Peng, Z., Letu, H.S., Wang, T.X., Shi, C., Zhao, C.F., Tana, G.G., Zhao, N.Z., Dai, T., Tang, R.L., Shang, H.Z., Shi, J.C., Chen, L.F., 2020. Estimation of shortwave solar radiation using the artificial neural network from Himawari-8 satellite imagery over China. J. Quant. Spectrosc. Radiat. Transf. 240.

Pinker, Frouin, Li, 1995. A review of satellite methods to derive surface shortwave irradiance. Remote Sens. Environ. 51 (1), 108–124.

Pinker, R.T., Ewing, J.A., Tarpley, J.D., 1985. The relationship between the planetary and surface net radiation. J. Clim. Appl. Meteorol. 24, 1262–1268.

Platnick, S., Meyer, K.G., King, M.D., Wind, G., Amarasinghe, N., Marchant, B., Arnold, G.T., Zhang, Z.B., Hubanks, P.A., Holz, R.E., Yang, P., Ridgway, W.L., Riedi, J., 2017. The MODIS Cloud Optical and Microphysical Products: Collection 6 Updates and Examples From Terra and Aqua. IEEE Trans. Geosci. Remote Sens. 55, 502–525.

Qin, J., Tang, W.J., Yang, K., Lu, N., Niu, X.L., Liang, S.L., 2015. An efficient physically based parameterization to derive surface solar irradiance based on satellite atmospheric products. J. Geophys. Res.-Atmos. 120, 4975–4988.

Ryu, Y., Jiang, C., Kobayashi, H., Detto, M., 2018. MODIS-derived global land products of shortwave radiation and diffuse and total photosynthetically active radiation at 5 km resolution from 2000. Remote Sens. Environ. 204, 812–825.

Schaaf, C.B., Gao, F., Strahler, A.H., Lucht, W., Li, X.W., Tsang, T., Strugnell, N.C., Zhang, X.Y., Jin, Y.F., Muller, J.P., Lewis, P., Barnsley, M., Hobson, P., Disney, M., Roberts, G., Dunderdale, M., Doll, C., d'Entremont, R.P., Hu, B.X., Liang, S., Privette, J.L., Roy, D., 2002. First operational BRDF, albedo nadir reflectance products from MODIS. Remote Sens. Environ. 83, 135–148.

Shi, Q., Liang, S., 2013. Characterizing the surface radiation budget over the Tibetan Plateau with ground-measured, reanalysis, and remote sensing data sets: 1. Methodology. J. Geophys. Res.-Atmosph. 118, 9642–9657.

Takenaka, H., Nakajima, T.Y., Higurashi, A., Higuchi, A., Takamura, T., Pinker, R.T., Nakajima, T., 2011. Estimation of solar radiation using a neural network based on radiative transfer. J. Geophy.l Res.-Atmosph. 116.

Tang, W.J., Qin, J., Yang, K., Liu, S.M., Lu, N., Niu, X.L., 2016. Retrieving high-resolution surface solar radiation with cloud parameters derived by combining MODIS and MTSAT data. Atmos. Chem. Phys. 16, 2543–2557.

Tang, W.J., Qin, J., Yang, K., Niu, X.L., Min, M., Liang, S.L., 2017a. An efficient algorithm for calculating photosynthetically active radiation with MODIS products. Remote Sens. Environ. 194, 146–154.

Tang, W.J., Yang, K., Sun, Z., Qin, J., Niu, X.L., 2017b. Global Performance of a Fast Parameterization Scheme for Estimating Surface Solar Radiation From MODIS Data. IEEE Trans. Geosci. Remote Sens. 55, 3558–3571.

Tang, W.J., Li, J., Yang, K., Qin, J., Zhang, G.Q., Wang, Y., 2019a. Dependence of remote sensing accuracy of global horizontal irradiance at different scales on satellite sampling frequency. Sol. Energy 193, 597–603.

Tang, W.J., Yang, K., Qin, J., Li, X., Niu, X.L., 2019b. A 16-year dataset (2000-2015) of high-resolution (3 h, 10 km) global surface solar radiation. Earth System Science Data 11, 1905–1915.

Tang, W.J., Yang, K., Qin, J., Li, J., Ye, J.G., 2021. How Accurate Are Satellite-Derived Surface Solar Radiation Products over Tropical Oceans? J. Atmos. Ocean. Technol. 38, 283–291.

Van Laake, P.E., Sanchez-Azofeifa, G.A., 2004. Simplified atmospheric radiative transfer modelling for estimating incident PAR using MODIS atmosphere products. Remote Sens. Environ. 91, 98–113.

Wang, D., 2012. High-level land product integration. In: Liang, S., Li, X., Wang, J. (Eds.), Advanced Remote Sesning: Terrestrial Information Extraction and Application. Academic Press.

Wang, D., Liang, S., 2014a. Improving LAI Mapping by Integrating MODIS and CYCLOPES LAI Products Using Optimal Interpolation. IEEE J. Selected Topics in Appl. Earth Observ. and Remote Sens. 7, 445–457.

Wang, D., Liang, S., 2014b. Mapping High-Resolution Surface Shortwave Net Radiation From Landsat Data. IEEE Geosci. Remote Sens. Lett. 11, 459–463.

Wang, H., Pinker, R.T., 2009. Shortwave radiative fluxes from MODIS: Model development and implementation. J. Geophys. Res.-Atmos. 114.

Wang, D., Liang, S., He, T., Cao, Y., Jiang, B., 2015a. Surface Shortwave Net Radiation Estimation from FengYun-3 MERSI Data. Remote Sens. 7, 6224–6239.

Wang, D., Liang, S., He, T., Shi, Q., 2015b. Estimation of daily surface shortwave net radiation from the combined MODIS data. IEEE Trans. Geosci. Remote Sens. 53, 5519–5529.

Wang, T., Fetzer, E.J., Wong, S., Kahn, B.H., Yue, Q., 2016. Validation of MODIS cloud mask and multilayer flag using CloudSat-CALIPSO cloud profiles and a cross-reference of their cloud classifications. J. Geophys. Res.-Atmos. 121, 11620–11635.

Wang, D., Liang, S., Zhang, Y., Gao, X., Brown, M., Jia, A., 2020. A New Set of MODIS Land Products (MCD18): Downward Shortwave Radiation and Photosynthetically Active Radiation. Remote Sens. 12.

Wei, Y., Zhang, X.T., Hou, N., Zhang, W.Y., Jia, K., Yao, Y.J., 2019. Estimation of surface downward shortwave radiation over China from AVHRR data based on four machine learning methods. Sol. Energy 177, 32–46.

Xie, Y., Sengupta, M., Dudhia, J., 2016. A Fast All-sky Radiation Model for Solar applications (FARMS): Algorithm and performance evaluation. Sol. Energy 135, 435–445.

Xiong, X., Sun, J., Barnes, W., Salomonson, V., Esposito, J., Erives, H., Guenther, B., 2007. Multiyear on-orbit calibration and performance of Terra MODIS reflective solar bands. IEEE Trans. Geosci. Remote Sens. 45, 879–889.

Zhang, X., Liang, S., Wild, M., Jiang, B., 2015. Analysis of surface incident shortwave radiation from four satellite products. Remote Sens. Environ. 165, 186–202.

Zhang, Y., He, T., Liang, S.L., Wang, D.D., Yu, Y.Y., 2018. Estimation of all-sky instantaneous surface incident shortwave radiation from Moderate Resolution Imaging Spectroradiometer data using optimization method. Remote Sens. Environ. 209, 468–479.

Zhang, X.T., Wang, D.D., Liu, Q., Yao, Y.J., Jia, K., He, T., Jiang, B., Wei, Y., Ma, H., Zhao, X., Li, W.H., Liang, S.L., 2019. An Operational Approach for Generating the Global Land Surface Downward Shortwave Radiation Product From MODIS Data. IEEE Trans. Geosci. Remote Sens. 57, 4636–4650.

Zhang, X.D., Zhou, J., Liang, S.L., Chai, L.N., Wang, D.D., Liu, J., 2020a. Estimation of 1-km all-weather remotely sensed land surface temperature based on reconstructed spatial-seamless satellite passive microwave brightness temperature and thermal infrared data. ISPRS J. Photogramm. Remote Sens. 167, 321–344.

Zhang, Y., Liang, S., He, T., Wang, D., Yu, Y., 2020b. Estimation of Land Surface Incident and Net Shortwave Radiation from Visible Infrared Imaging Radiometer Suite (VIIRS) Using an Optimization Method. Remote Sens. 12, 4153.

Zhang, Y., Liang, S., He, T., Wang, D., Yu, Y., Ma, H., 2021. Estimation of Land Surface Incident Shortwave Radiation From Geostationary Advanced Himawari Imager and Advanced Baseline Imager Observations Using an Optimization Method. IEEE Transcations on Geoscience and Remote Sensing. (in press).